Nuclear Materials and Energy 33 (2022) 101249

Contents lists available at ScienceDirect

Nuclear Materials and Energy

journal homepage: www.elsevier.com/locate/nme

Retention of deuterium in beryllium: A combined investigation using TDS, ERDA and EBS

C. Cupak [a,*], E. Pitthan [b], M.V. Moro [b], M. Fellinger [a], D. Primetzhofer [b], F. Aumayr [a]

[a] Institute of Applied Physics, TU Wien, Fusion@ÖAW Wiedner Hauptstraße 8-10/E134, 1040 Vienna, Austria
[b] Department of Physics and Astronomy, Uppsala University, Box 516, 751 20 Uppsala, Sweden

ARTICLE INFO

Keywords:
Deuterium
Beryllium
Retention
Ion beam analysis
Temperature desorption spectroscopy

ABSTRACT

We have studied the retention of deuterium in beryllium, implanted with an energy of 500 eV/D, using a combination of thermal desorption spectroscopy, elastic recoil detection analysis and elastic backscattering spectroscopy. The parallel use of these techniques allowed us to directly quantify the absolute deuterium content reduction of the sample for specific desorption peaks observed during thermal annealing. In addition, the presence of a beryllium oxide surface layer was observed, despite sputter-cleaning of the sample was initially conducted *in-situ*. A main result was that ~85 % of the retained deuterium got released during the primary desorption peak at 400 K. A smaller, secondary desorption peak was identified at 540 K. All deuterium could be removed from the Be sample by heating it to a temperature of 800 K.

1. Introduction

Retention of hydrogen isotopes in first wall materials of nuclear fusion devices is an important scientific topic, since the capture of fuel atoms from the plasma affects both the efficiency and the safety of future fusion reactors. On the one hand, the hydrogen isotope tritium is very rare and needs to be harvested from breeding blankets and recycled on-site with high technological efforts [1–3]. Thus, it would be detrimental if a large fraction of these rare fuel atoms is retained in the wall of a reactor. On the other hand, also an enhanced erosion due to chemically assisted sputtering was observed, e.g., for beryllium (Be) Plasma-Facing-Components (PFCs) with retained hydrogen isotopes [4]. Furthermore, the retention of tritium is also of concern for confinement of radioactive inventory, especially if tritium diffuses through the first wall materials into the cooling medium [5–8]. Also the retention within nanoscale dust particles eroded from first wall materials forms a safety issue, since this radioactive dust can cause severe harm to the environment and humans, if emitted, e.g., in the event of a large reactor malfunction or maintenance [9,10]. Despite large efforts taken in this field, comprehensive studies on hydrogen isotope retention in first wall materials remain of interest, to successfully predict the properties of possible first wall materials during application in future fusion reactors.

Since tritium is rare and radioactive, laboratory studies often utilise non-radioactive hydrogen isotopes like deuterium (D) for retention experiments. A large number of studies considering both experiments and numerical approaches was performed for the retention of D in tungsten (W), which is the most promising material foreseen for the divertor region of a nuclear fusion reactor [11]. Beyond the W divertor, Be is foreseen as a main vessel material [12,13] and also as a neutron multiplier within the tritium breeding blankets [14] in ITER, currently under construction in France. Be migration from the main chamber towards the divertor can be expected, which also causes co-deposition of fuel atoms and therefore contributes significantly to the overall fuel retention [15,16]. In addition, the Be components in the reactor vessel may also be directly exposed to high particle fluxes from the plasma, especially during transient events like an Edge Localised Mode (ELM) [17,18]. Similar to the comprehensive number of studies already found in literature [19–25] on this topic, the investigation of D retention in Be due to direct ion implantation is therefore also a main motivation for this work.

In the last decades, experimental investigation of hydrogen isotope retention in materials was mostly obtained by two distinctive experimental methods: Temperature Desorption Spectroscopy (TDS), sometimes also referred to as Temperature Programmed Desorption (TPD), or Ion Beam Analysis (IBA). For the former, a specimen is continuously heated, while the time-dependent signal from a Residual Gas Analyser (RGA) for certain gas species within the experimental chamber is inspected [26]. This method allows, e.g., to identify TDS peaks from pre-implanted samples at certain temperatures, which correspond to specific binding energies of retained atoms in a trapping site. Alternatively, probing ion beams with MeV kinetic energy can be

* Corresponding author.
E-mail address: cupak@iap.tuwien.ac.at (C. Cupak).

https://doi.org/10.1016/j.nme.2022.101249
Received 20 June 2022; Received in revised form 1 September 2022; Accepted 8 September 2022
Available online 14 September 2022

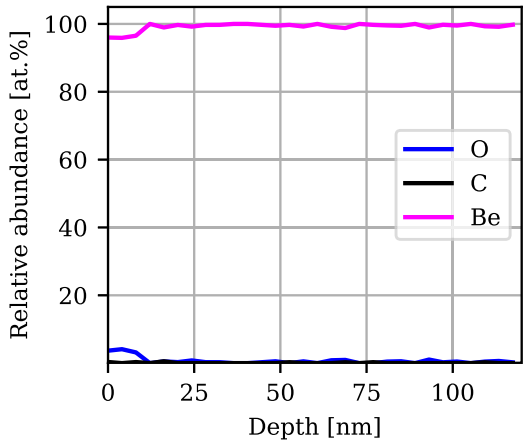

Fig. 1. Depth profile of a Be sample obtained by ToF-E ERDA, conducted *ex-situ* prior the TDS experiment. The relative atomic abundance is plotted against the depth in the sample from the surface.

used in IBA to quantify total abundances of retained hydrogen isotopes in relevant plasma facing materials [27].

An *in-situ* combination of D implantation, followed by immediate TDS and IBA within the same experiment is favourable, to avoid problems caused by hydrogen isotope exchange or oxidation due to sample transport at atmosphere [27]. Such a combination was, e.g., recently demonstrated in a study on D retention in W [28]. A main aspect of our current work was therefore to conduct such an experimental approach also for studying D retention in polycrystalline Be. The key goal was to quantify the respective amount of D released during certain TDS peaks, which allows to directly assess the contribution of individual trapping site types to the overall retention capacity.

2. Materials and methods

Polycrystalline Be samples were used in this study as samples for the D retention experiments. The dimensions of the square-shaped platelets were $10 \times 10 \times 1$ mm^3. Before the experiments, these samples were cleaned in an ultrasonic bath with isopropanol to remove surface contaminations. Afterwards, the samples were characterised by means of ToF-E ERDA, using a probing ion beam of 36 MeV I^{8+} [29]. Besides a small O content within the first 10 nm from the surface and very small traces of C, the samples were found to consist of practically pure Be (see Fig. 1).

For the D retention experiments in this study, the SIGMA setup at Uppsala University was utilised [30], which is connected to a 5-MV NEC-15SDH-2 Tandem accelerator [31]. It incorporates many options for sample preparation and modification under Ultra High Vacuum (UHV) conditions and further *in-situ* investigations with various IBA based techniques, e.g., EBS, Particle Induced X-ray Emission (PIXE) or Elastic Recoil Detection Analysis (ERDA). In addition, annealing of samples with an e^--beam heating system (temperature increase rates down to 0.1 K/s) and simultaneous residual gas analysis allow to conduct TDS measurements. Also, a combination of IBA with TDS is possible and was recently demonstrated in a study on D retention in polycrystalline W samples [28]. As a first step, the Be samples were fixed on transferable sample holders and loaded in the load-lock chamber in the SIGMA setup. To ensure homogeneous heat distribution during annealing and to reduce noise at the detectors caused by light emission from the e^--beam heater filament, a sufficiently large W foil with approximately 100 μ m thickness was mounted between sample holder and Be sample. To monitor the temperature during annealing, a K-type thermocouple was attached directly to the sample, which was furthermore cross-checked by a pyrometer (PV 11-Keller HCW) at 1000 °C. For the TDS measurements, a Pfeiffer QMG 250 F1 PrismaPro RGA was used. The signal for D_2, being the main gas species of interest, was also calibrated with a Pfeiffer PKR 361 pressure gauge.

Prior to the D implantation, a Prevac IS40 ion source was used to sputter-clean the sample with 1 keV Ar^+ ions under 60° incidence angle for at least 45 min (~20 nm erosion), to remove surface contaminants. Afterwards, the sample was exposed to a D ion beam with 1 keV under 7° incidence angle (to prevent eventual channelling effects) from the same ion source for a desired time (see schematic sketch in Fig. 2 left). The ion beam size was approximately 1 cm^2, while the stability of the ion current impinging on the sample could be monitored during irradiation [32]. The average D ion current was 5.7 μA and therefore, a flux of about 3.5×10^{13} ions/cm^2/s was determined. In agreement to previous studies with the SIGMA setup, the ion beam was assumed to consist of a mixture with 7 % D^+ and 93 % D_2^+ ions [28,33].

Simulations with the Binary Collision Approximation (BCA) code SDTrimSP [34], employing a user-friendly GUI [35], allowed to assess the implantation range of the D^+ and D_2^+ ions in Be (see Fig. 2 right). Here, it was assumed that the 1000 eV D_2^+ ions dissociate into atomic D with 500 eV kinetic energy upon impact, causing individual collision cascades. While the 1000 eV D^+ ions have a substantially larger range up to 500 Å, their relative contribution is small, compared to the range of the dominant (dissociated) 500 eV D^+ projectiles. Since most ions were stopped within the first 400 Å, it can be assumed that this range is the relevant implantation zone (see Fig. 2). SDTrimSP also calculated a reflection coefficient of 7.3 %. In addition, D outgassing from the sample during implantation cannot be prevented. Therefore, all D implantation fluences declared in this manuscript correspond to nominal doses.

During the implantation process, the temperature of the SIGMA setup was slightly increased to about 60 °C to mitigate adsorbate coverage on the inner chamber walls. This rise was achieved by soft baking of the whole setup, which therefore also led to a corresponding rise of the Be sample temperature during implantation. After the desired implantation time, the irradiated sample was transferred to the storage section in the load-lock chamber without breaking the vacuum. Then, the goniometer head in the experimental section was pre-annealed to about 100 °C for 1 h to further reduce adsorbates. This should prevent unfavourable contributions to the TDS spectrum during sample annealing. No D_2 outgassing could be observed by our RGA during this pre-annealing step.

After the pre-annealing, the D irradiated sample was again moved to the experimental section of SIGMA and oriented for the simultaneous IBA and TDS investigation (see schematic sketch in Fig. 2 left). A dwell time of approximately 1.5 h passed between implantation and the actual start of measurements. An energy of 3.037 MeV was selected for the probing $^4He^+$ ion beam in this study, which had a spot size of about 2 mm^2. The reason for this particular energy will be explained below. With respect to the incoming beam direction, the sample was rotated towards an incidence angle of 70°. This allowed to use in total three Passivated Implanted Planar Silicon (PIPS) detectors: two individual ERDA detectors for investigating H and D contents and spectra normalisation, and an EBS detector for investigating the O content. The primary ERDA detector (named here as ERDA-1, with a solid angle of 3.46×10^{-3} sr) was located at a scattering angle of 30° and the secondary one (named as ERDA-2, with a solid angle of 3.78×10^{-3} sr) at a scattering angle of 40°. The former was equipped with an Al-foil (thickness 10.3 μm) to prevent detection of scattered $^4He^+$ or recoiled Be or O atoms. This detector therefore only received H or D recoil atoms from the sample. Since fluctuations of the primary $^4He^+$ ion beam were possible, also a method for normalisation of the recorded spectra was required for further data analysis. In similar studies focusing on samples consisting of heavier elements like tungsten, an option was to use the signal from a PIXE detector to monitor any primary ion beam current variations [28]. However, the much lighter Be atoms in our sample excluded utilisation of X-ray based techniques. Also approaches

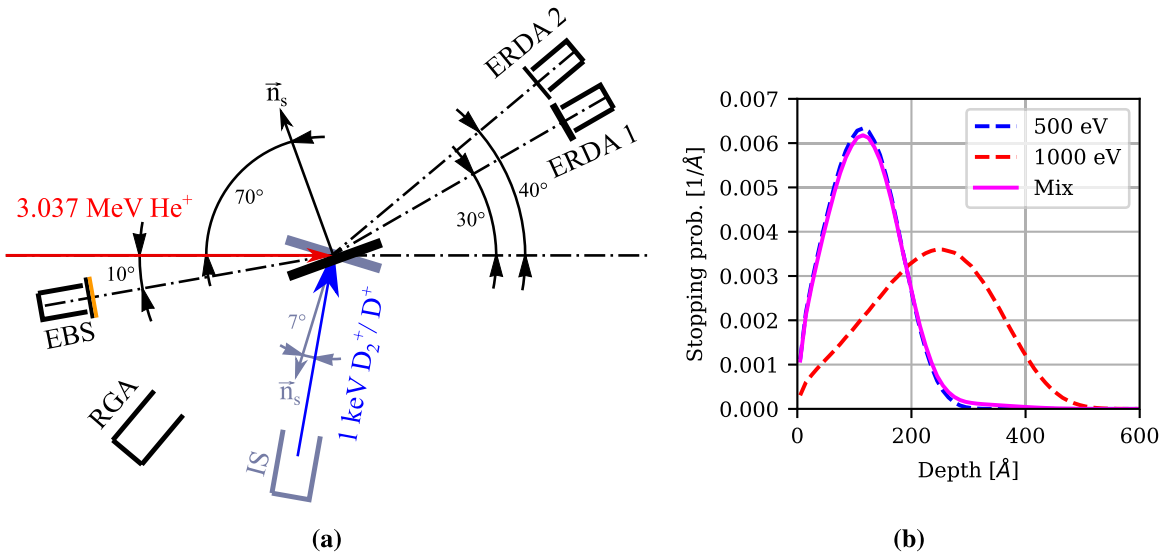

Fig. 2. Left: Schematic sketch of the setup geometry. The grey configuration was used during 1 keV D^+/D_2^+ implantation with the ion source (IS). The black configuration was used during the parallel IBA and TDS measurements with the 3.037 MeV $^4He^+$ beam. **Right:** D ion ranges simulated by SDTrimSP [34] for 500 eV (blue) and 1000 eV (red) on pure Be under 7° incidence angle, assuming static conditions. Also, the total profile for the assumed mixture of D^+ and D_2^+ emitted from the ion source is plotted (magenta). (For interpretation of the references to colour in this figure legend, the reader is referred to the web version of this article.)

based on classic Rutherford backscattering were difficult due to the very low backscattering energy of primary $^4He^+$ projectiles, which led to the choice of a secondary ERDA detector as normalisation option. This detector was equipped with a thinner Al-foil (6.61 μm) causing the detected spectrum to originate mostly from scattered He projectiles. Since this signal was proportional to the current of the primary $^4He^+$ ion beam, which was measured prior and after each measurement by means of a Faraday Cup, this data allowed to monitor current fluctuations and to normalise the spectra recorded by the other detectors. A representative spectrum obtained from a D implanted Be sample can be seen in Fig. 3 left. The normalised counts of H and D recoil atoms are plotted against the detector energy channel. In this plot, it can be seen that the signals originating from H and D are well separated in energy and therefore the D signal is not affected by the low, but inevitable H contamination. Also, depth scales are added to this figure, to visualise the probing range of the 3.037 MeV $^4He^+$ beam. It has to be mentioned that the experimental conditions for IBA were primarily selected to achieve a large overall range, i.e., deeper than 400 nm. With this, the total D content in the sample can be quantified well beyond the implantation zone, despite depth resolution being limited. The selected energy furthermore supported the usage of an EBS detector (located at −10° respective the incoming probing beam direction and a solid angle of 2.08 × 10^{-3} sr) for the investigation of the total surface O amount. The primary $^4He^+$ ion beam energy of 3.037 MeV allowed favourable resonant elastic scattering with O [36,37]. This enabled us to significantly increase the oxygen scattering cross-section for the surface near region (several 10 nm), since the cross-section decreases dramatically for non-resonant projectile energies (i.e., as $^4He^+$ ions are continuously stopped by transmission through the material). Still, any O contamination of the bulk material would be visible, despite the lower scattering cross-sections. The EBS detector was also covered by an absorber-foil (~139 nm Au on a 44 nm C foil), to reduce noise caused by light emitted from the e^--beam heater during annealing. A representative spectrum is shown in Fig. 3 right. The experimental spectra from ERDA and EBS detectors could be well reproduced using the software SIMNRA [38], by considering the scattering geometry, stopping power values from SRIM [39], and elastic recoil cross sections for $^1H(\alpha,p)^4He$ from SigmaCalc [40] and $D(^4He,D)^4He$ from Han et al. [41]. For the non-Rutherford resonant cross section of $^{16}O(\alpha,\alpha_0)^{16}O$, again the SigmaCalc database was used. In addition, besides a pure Be bulk composition, a mixed top layer consisting of H, D and Be with approximately 40 nm thickness was considered for the sample, in agreement with the implantation range simulated by SDTrimSP. Since a complete saturation of the implantation process was assumed for the fluence applied in this study, a uniform distribution of D was approximated in this layer. Furthermore, also a uniform abundance of O was added within the first 7 nm from the surface, which we found to reproduce the width of our experimental EBS spectrum best. By fine-tuning of the elemental abundances in these top layers, the reconstructed SIMNRA spectra could be fitted to the experimental data (magenta in Fig. 3), which in turn allowed to assess the total areal density of these species in the experimental sample. All IBA detectors recorded continuously throughout the TDS procedure. By splitting the data into discrete sets with 100 s measurement time each, changes in the total areal density for H, D and O over time or sample temperature could be monitored quantitatively.

3. Results and discussion

For the combined TDS and IBA experiment, the Be sample was first implanted with 500 eV/D for about 15.5 h to achieve a nominal D fluence of 4.0 × 10^{18} D/cm^2. Initial ERDA measurements revealed a total areal D content of 8.36 × 10^{16} D/cm^2 in the sample after implantation. Since the static SDTrimSP simulations predicted an implantation range of ~40 nm (compare Fig. 2 right) and no D could be detected in larger depths (compare Fig. 3 left), it was assumed that only the implantation zone is relevant for D trapping in our studied case.

By assuming an initially pure Be target in the first 40 nm, the total areal D content after implantation can be furthermore expressed as a relative atomic D abundance of up to 14.5 at.% in this region. It must be mentioned that due to the rather limited depth resolution, no precise verification of the implantation depth was possible.

For the annealing experiment, all ERDA, EBS detectors and the RGA were continuously recording throughout TDS up to 800 K. A temperature increase rate of ~0.12 K/s was followed. We generally observed a reappearance of surface O contamination after D implantation, even though sputter-cleaning was performed initially to reduce O on the surface. It is well known from literature that pure Be acts as a good oxygen getter material in UHV [42], which probably led to the formation of a BeO surface layer *in-situ*, despite reasonable vacuum conditions (~1.0 × 10^{-8} mbar base pressure) during our experiments.

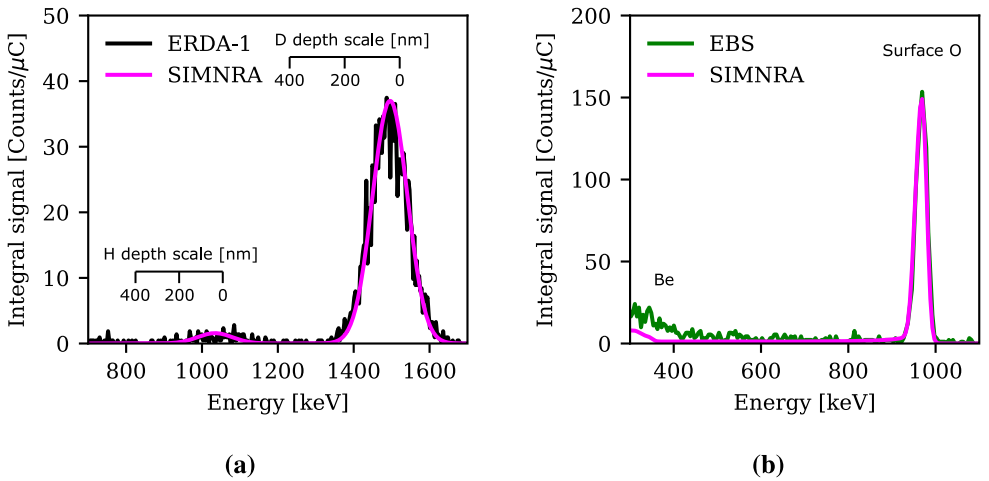

Fig. 3. Left: Representative normalised spectrum of the primary ERDA detector (ERDA-1, black) measured for a D implanted Be sample. **Right:** Representative normalised spectrum of the EBS detector (green) for the same sample. The resonant $^{16}O(\alpha,\alpha_0)^{16}O$ reaction is very surface sensitive, therefore no depth scale bars are given. For both ERDA and EBS, a reconstructed spectrum from SIMNRA (magenta) is shown [38]. Similar spectra were obtained for each 100 s time step of the continuous measurements during sample annealing. (For interpretation of the references to colour in this figure legend, the reader is referred to the web version of this article.)

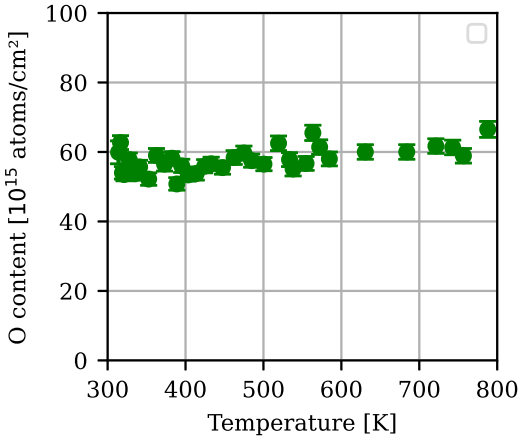

Fig. 4. Surface O content measured by EBS on the Be sample during the TDS experiment. The total areal surface content of O is plotted against the sample temperature up to 800 K.

The O content measured by EBS was found to be very stable throughout the TDS measurement up to high temperatures, as can be seen in Fig. 4. This supports the hypothesis of BeO formation, as it is a very stable compound (melting temperature 2823 K [43,44]). This effect was also reproduced for a Be twin sample with a very similar O content. It is plausible that such unintended BeO formation can also happen in a nuclear fusion device, as it also occurred in other experiments reported in literature [45].

The calibrated RGA data for D_2 (4 amu) is plotted in Fig. 5 (top), while the corresponding ERDA based data for the total D content is shown in the plot below, both as a function of increasing sample temperature. Initially, a short spike in the RGA signal can be seen at a temperature of about 330 K (marked by X). This event coincided with activating the high voltage supply of the e^--beam heater and had no detectable effect on the retained D abundance measured by ERDA. Therefore, we discarded this event as an artefact. It also has to be mentioned that a short interruption of the sample heating occurred at around ~380 K, since one of the IBA detectors needed to be reseted due to noise before the experiment could be continued. To distinguish these two heating phases, they are labelled in different colours in the TDS plot in Fig. 5, where the orange and red colours correspond to the data before and after interruption, respectively. The first phase already led to a partial emission of the D content. Still, the trends of the orange and red TDS signals overlap very well and lead to a primary TDS peak (marked by 1) close to 400 K, which coincided with a rapid drop in the D content to about 12.5×10^{15} D/cm^2 as seen in the ERDA data (Fig. 5 bottom). The interruption caused the height of the primary TDS peak to appear relatively low. For comparison, another TDS measurement with a Be twin sample exposed to the same nominal D fluence was conducted, where a primary peak at almost the same temperature, but with correspondingly higher amplitude was observed (not shown). At higher temperatures, our data indicate a correlation of a smaller, secondary TDS peak at 540 K (marked by 2) with a second drop in the D content down to 6×10^{15} D/cm^2, while the width of this TDS peak is significantly broader and some fluctuations on the rising slope can be recognised. Then, a continuous decrease towards even smaller amounts of retained D is found for increasing temperatures up to 800 K (marked by 3).

In the following, the results of our experiment are discussed. At first, a focus is put on the total D areal density obtained after implantation. By comparing the nominal incident fluence (4.0×10^{18} D/cm^2) and the retained amount of D (8.36×10^{16} D/cm^2), it can be estimated that only 2 % of the impinging D atoms were actually retained. This observation indicates that the Be sample was irradiated significantly beyond saturation, in agreement to findings reported in literature [19,20,25]. Furthermore, the amount of totally retained D areal density after saturated implantation corresponds well to previous results in other studies [22,25]. For example, W.R. Wampler observed that during 500 eV/D irradiation, saturation occurred already for incident fluences above 5×10^{17} D/cm^2, where a very similar retained D content of ~9.0×10^{16} D/cm^2 was quantified [24].

Next, a focus is put on the primary TDS peak found in the D_2 signal of the RGA (marked by 1). The observed temperature of 400 K is principally in good agreement with values reported in literature [19–23]. For instance, M. Eichler also identified TDS peaks close to 400 K for Be samples if they were irradiated with incident D fluences exceeding 3×10^{17} D/cm^2 [25]. Discrepancies of some 10 K are expectable for independent TDS experiments, since they often rely on thermocouple measurements, which are prone for some offset errors due to thermal contact issues. During the event associated with the primary TDS peak, our ERDA measurements carried out simultaneously with TDS showed that ~85 % of the initially retained D was released. Following the argumentation by Reinelt et al. [20], we interpret this low temperature TDS peak to originate from D retention in low-energy traps within a highly amorphised region in the implantation zone, which develops

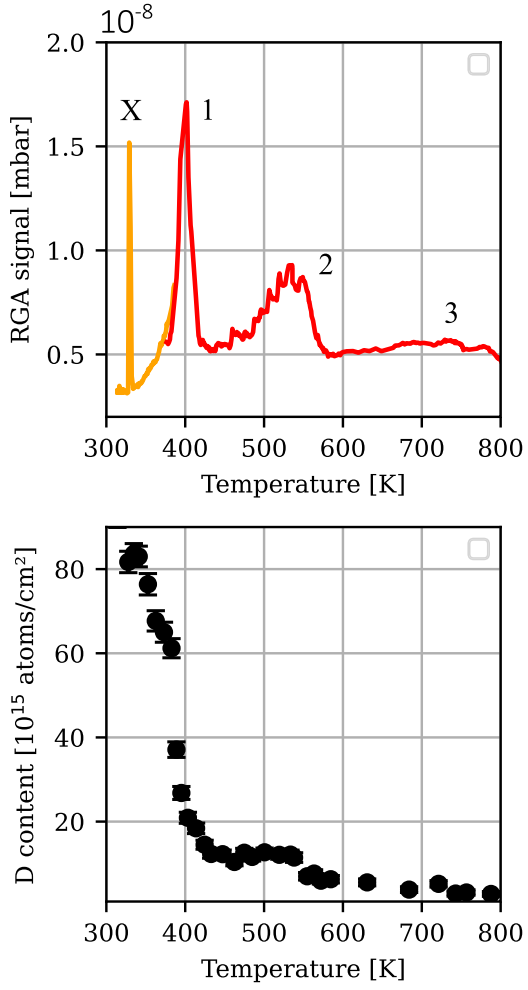

Fig. 5. TDS (**top**, calibrated 4 amu signal) and ERDA (**bottom**, total D content) data versus sample temperature during the experiment: The Be sample was initially irradiated with a fluence of 4.0×10^{18} D/cm^2, before parallel IBA and TDS was performed up to 800 K.

beyond a certain fluence. For the secondary TDS peak at 540 K (marked by 2), an additional, but smaller decrease by another 8 % of the initially retained D was found by ERDA. The small fluctuations on the rising slope of the second TDS peak coincided with incremental power increases of the heating system. This observation suggests that radiative heating led to desorption of D adsorbates from surrounding parts in the UHV chamber, therefore contributing to the TDS signal, while ERDA data was not affected yet. Generally, the width and magnitude of this TDS peak appear similar to the secondary TDS peak found by Oberkofler et al. [19] in pure Be, while in our case, this signal was observed already at significantly lower temperature. It has to be mentioned, that a slightly higher D energy (600 eV/D) and a faster heating ramp (0.7 K/s) were used in [19], which could have affected the TDS peak position. In literature, the high-temperature TDS peak is connected to degassing from local defects in the Be lattice, which can be present naturally or by generation during ion bombardment itself [20]. Thus, this peak is also expectable in cases with much lower applied D fluence as in our study. At higher temperatures, ERDA shows that the remaining 7 % were then continuously outgassing, dropping below 2.5×10^{15} D/cm^2 at 800 K. This decrease of D content corresponds to a very broad but low plateau in the TDS data (marked by 3 in the RGA signal), which was similarly found by Oberkofler et al. for a BeO sample [19], therefore suggesting also to be the reason for these trends in our study. Since the BeO surface layer developed already during the D implantation, it is expected that ion-induced displacement damage within the BeO layer provided the relevant trapping sites for this TDS peak, as discussed by Anderl et al. [46]. Since ERDA did show that practically no D was left in our sample at the highest temperature of 800 K, the remaining D signals from the RGA at this temperature are again attributed to D desorption caused by radiative heating of the vacuum chamber walls. The quantification of the D content during heating of the sample is therefore a major advantage of our combined TDS/ERDA approach, in comparison to studies focusing on TDS exclusively.

4. Summary and conclusion

In the course of this study, IBA and TDS were employed *in-situ* and simultaneously for an investigation of D retention in polycrystalline Be bulk samples. The SIGMA setup enabled D implantation with 500 eV/D energy up to a total incident fluence of 4.0×10^{18} D/cm^2, while ERDA showed that only 2 % of this D amount were finally retained in the sample. Annealing was performed towards a temperature of 800 K. Besides the investigation of the outgassing characteristics with an RGA, ERDA allowed a direct quantification of the remaining D content in the sample and thus enabled to correlate TDS peak events with a certain release of D inventory. In addition, this approach allowed to separate TDS contributions which were caused by peripheral sources. Besides, the surface O content could be monitored by means of EBS, which revealed an almost constant O abundance near the sample surface. This observation suggests that formation of a stable BeO surface layer occurred, despite initial sputter-cleaning of the sample was performed under UHV conditions. For D_2, a dominant TDS peak was found around 400 K, in good agreement with literature values. The simultaneous measurements with ERDA showed that the majority of D content (i.e., ~85 %) was released in this event. A second TDS peak at 540 K led to another small reduction in the total D content, before the remainder got emitted continuously until 800 K were reached. For the overall shape of the TDS spectrum, contributions from both the pure Be bulk and the surface BeO layer are suggested. These results demonstrate the capabilities of the SIGMA setup for *in-situ* investigations of retention mechanisms in first wall materials.

CRediT authorship contribution statement

C. Cupak: Conceptualization, Data curation, Formal analysis, Investigation, Visualization, Writing – original draft. **E. Pitthan:** Data curation, Formal analysis, Investigation, Writing – review & editing. **M.V. Moro:** Conceptualization, Investigation, Methodology, Writing – review & editing. **M. Fellinger:** Investigation, Writing – review & editing. **D. Primetzhofer:** Conceptualization, Funding acquisition, Methodology, Project administration, Resources, Supervision, Writing – review & editing. **F. Aumayr:** Conceptualization, Funding acquisition, Project administration, Supervision, Writing – review & editing.

Data availability

Data will be made available on request.

Acknowledgements

This work has been carried out within the framework of the EUROfusion Consortium, funded by the European Union via the Euratom Research and Training Programme (Grant Agreement No 101052200—EUROfusion). Views and opinions expressed are however those of the author(s) only and do not necessarily reflect those of the European Union or the European Commission. Neither the European Union nor the European Commission can be held responsible for them. Financial support has also been provided by KKKÖ (commission for the coordination of fusion research in Austria at the Austrian Academy of

Sciences - ÖAW). Support of the operation of the tandem accelerator at Uppsala University, Sweden by VR-RFI (contract #2019-00191) is gratefully acknowledged. The authors acknowledge TU Wien Bibliothek for financial support through its Open Access Funding Programme. Furthermore, the authors highly appreciate the help of Timo Dittmar (FZ Jülich, Germany) regarding sample acquisition.

Declaration of competing interest

The authors declare that they have no known competing financial interests or personal relationships that could have appeared to influence the work reported in this paper.

References

[1] L. Giancarli, M. Abdou, D. Campbell, V. Chuyanov, M. Ahn, M. Enoeda, C. Pan, Y. Poitevin, E. Rajendra Kumar, I. Ricapito, Y. Strebkov, S. Suzuki, P. Wong, M. Zmitko, Overview of the ITER TBM program, Fusion Eng. Des. 87 (2012) 395–402, http://dx.doi.org/10.1016/j.fusengdes.2011.11.005.

[2] I. Cristescu, F. Priester, D. Rapisarda, A. Santucci, M. Utili, Overview of the tritium technologies for the EU DEMO breeding blanket, Fusion Sci. Technol. 76 (2020) 446–457, http://dx.doi.org/10.1080/15361055.2020.1716456.

[3] T. Tanabe, Tritium: Fuel of Fusion Reactors, Vol. 1, Springer, Tokyo, 2017.

[4] S. Brezinsek, M. Stamp, D. Nishijima, D. Borodin, S. Devaux, K. Krieger, S. Marsen, M. O'Mullane, C. Bjoerkas, A. Kirschner, JET EFDA contributors, Study of physical and chemical assisted physical sputtering of beryllium in the JET ITER-like wall, Nucl. Fusion 54 (2014) 103001, http://dx.doi.org/10.1088/0029-5515/54/10/103001.

[5] B. Bornschein, C. Day, D. Demange, T. Pinna, Tritium management and safety issues in ITER and DEMO breeding blankets, Fusion Eng. Des. 88 (2013) 466–471, http://dx.doi.org/10.1016/j.fusengdes.2013.03.032.

[6] I. Cristescu, I. Cristescu, L. Doerr, M. Glugla1, D. Murdoch, Tritium inventories and tritium safety design principles for the fuel cycle of ITER, Nucl. Fusion 47 (2007) S458, http://dx.doi.org/10.1088/0029-5515/47/7/S08.

[7] K. Katayama, Y. Someya, K. Tobita, H. Nakamura, H. Tanigawa, M. Nakamura, N. Asakura, K. Hoshino, T. Chikada, Y. Hatano, S. Fukada, Estimation of tritium permeation rate to cooling water in fusion DEMO condition, Fusion Sci. Technol. 71 (2017) 261–267, http://dx.doi.org/10.1080/15361055.2017.1288423.

[8] K. Katayama, T. Matsumoto, A. Ipponsugi, Y. Someya, Tritium permeation from tritiated water to water through inconel, J. Nucl. Mater. 565 (2022) 153723, http://dx.doi.org/10.1016/j.jnucmat.2022.153723.

[9] T. Otsuka, S. Masuzaki, N. Ashikawa, Y. Hatano, Y. Asakura, T. Suzuki, T. Suzuki, K. Isobe, T. Hayashi, M. Tokitani, Y. Oya, D. Hamaguchi, H. Kurotaki, R. Sakamoto, H. Tanigawa, M. Nakamichi, A. Widdowson, M. Rubel, Tritium retention characteristics in dust particles in JET with ITER-like wall, Nucl. Mater. Energy 17 (2018) 279–283, http://dx.doi.org/10.1016/j.nme.2018.11.001.

[10] G. Mazzini, T. Kaliatka, M. Porfiri, Tritium and dust source term inventory evaluation issues in the European DEMO reactor concepts, Fusion Eng. Des. 146, Part A (2019) 510–513, http://dx.doi.org/10.1016/j.fusengdes.2019.01.008.

[11] T. Hirai, S. Panayotis, V. Barabash, C. Amzallag, F. Escourbiac, A. Durocher, M. Merola, J. Linke, T. Loewenhoff, G. Pintsuk, M. Wirtz, I. Uytdenhouwen, Use of tungsten material for the ITER divertor, Nucl. Mater. Energy 9 (2016) 616–622, http://dx.doi.org/10.1016/j.nme.2016.07.003.

[12] M. Rubel, V. Bailescu, J. Coad, T. Hirai, J. Likonen, J. Linke, C.P. Lungu, G. Matthews, L. Pedrick, V. Riccardo, P. Sundelin, E. Villedieu, JET-EFDA Contributors, Beryllium plasma-facing components for the ITER-like wall project at JET, J. Phys. Conf. Ser. 100 (2008) 062028, http://dx.doi.org/10.1088/1742-6596/100/6/062028.

[13] A. Raffray, B. Calcagno, P. Chappuis, Z. Fu1, A. Furmanek, C. Jiming, D.-H. Kim, S. Khomiakov, A. Labusov, A. Martin, M. Merola, R. Mitteau, S. Sadakov, M. Ulrickson, F. Zacchia, Contributors from the Blanket Integrated Product Team, The ITER blanket system design challenge, Nucl. Fusion 54 (2014) 033004, http://dx.doi.org/10.1088/0029-5515/54/3/033004.

[14] S. Konishi, M. Enoeda, M. Nakamichi, T. Hoshino, A. Ying, S. Sharafat, S. Smolentsev, Functional materials for breeding blankets—status and developments, Nucl. Fusion 57 (2017) 092014, http://dx.doi.org/10.1088/1741-4326/aa7e4e.

[15] S. Brezinsek, A. Widdowson, M. Mayer, V. Philipps, P. Baron-Wiechec, J. Coenen, K. Heinola, A. Huber, J. Likonen, P. Petersson, M. Rubel, M. Stamp, D. Borodin, J. Coad, A. Carrasco, A. Kirschner, S. Krat, K. Krieger, B. Lipschultz, C. Linsmeier, G. Matthews, K. Schmid, JET contributors, Beryllium migration in JET ITER-like wall plasmas, Nucl. Fusion 54 (2014) 103001, http://dx.doi.org/10.1088/0029-5515/54/10/103001.

[16] A. Hakola, K. Heinola, K. Mizohata, J. Likonen, C. Lungu, C. Porosnicu, E. Alves, R. Mateus, I. Bogdanovic Radovic, Z. Siketic, V. Nemanic, M. Kumar, C. Pardanaud, R. P., EUROfusion WP PFC Contributors, Effect of composition and surface characteristics on fuel retention in beryllium-containing co-deposited layers, Phys. Scr. T171 (2020) 014038, http://dx.doi.org/10.1088/1402-4896/ab4be8.

[17] A. Herrmann, T. Eich, V. Rohde, C. Fuchs, J. Neuhauser, ASDEX Upgrade team, Power deposition outside the divertor in ASDEX upgrade, Plasma Phys. Control. Fusion 46 (2004) 971, http://dx.doi.org/10.1088/0741-3335/46/6/004.

[18] B. Spilker, J. Linke, G. Pintsuk, M. Wirtz, Experimental study of ELM-like heat loading on beryllium under ITER operational conditions, Phys. Scr. 2016 (2016) T167, http://dx.doi.org/10.1088/0031-8949/T167/1/014024.

[19] M. Oberkofler, C. Linsmeier, Deuterium release from implanted beryllium and beryllium oxide, J. Nucl. Mater. 415 (2011) S724–S727, http://dx.doi.org/10.1016/j.jnucmat.2010.11.015.

[20] M. Reinelt, A. Allouche, M. Oberkofler, C. Linsmeier, Retention mechanisms and binding states of deuterium implanted into beryllium, New J. Phys. 11 (2009) 043023, http://dx.doi.org/10.1088/1367-2630/11/4/043023.

[21] R. Stadlmayr, P.S. Szabo, H. Biber, H.R. Koslowski, E. Kadletz, C. Cupak, R.A. Wilhelm, M. Schmid, F. Aumayr, A high temperature dual-mode quartz crystal microbalance technique for erosion and thermal desorption spectroscopy measurements, Rev. Sci. Instrum. 91 (2020) 125104, http://dx.doi.org/10.1063/5.0012028.

[22] A. Haasz, J. Davis, Deuterium retention in beryllium, molybdenum and tungsten at high fluences, J. Nucl. Mater. 241–243 (1997) 1076–1081, http://dx.doi.org/10.1016/S0022-3115(97)80197-3.

[23] A. Markin, V. Chernikov, S. Rybakov, A. Zakharov, Thermal desorption of deuterium implanted into beryllium, J. Nucl. Mater. 233–237 (1996) 865–869, http://dx.doi.org/10.1016/S0022-3115(96)00044-X.

[24] W. Wampler, Retention and thermal release of deuterium implanted in beryllium, J. Nucl. Mater. 123 (1984) 1598–1602, http://dx.doi.org/10.1016/0022-3115(84)90310-6.

[25] M. Eichler, Investigation of hydrogen isotope retention mechanisms in beryllium: High resolution TPD measurements, Nucl. Mater. Energy 19 (2019) 440–444, http://dx.doi.org/10.1016/j.nme.2019.03.018.

[26] P. Redhead, Thermal desorption of gases, Vacuum 12 (1962) 203–211, http://dx.doi.org/10.1016/0042-207X(62)90978-8.

[27] M. Mayer, S. Möller, M. Rubel, A. Widdowson, S. Charisopoulos, T. Ahlgren, E. Alves, G. Apostolopoulos, N. Barradas, S. Donnelly, S. Fazinić, K. Heinola, O. Kakuee, H. Khodja, A. Kimura, A. Lagoyannis, M. Li, S. Markelj, M. Mudrinic, P. Petersson, I. Portnykh, D. Primetzhofer, P. Reichart, D. Ridikas, T. Silva, S. Gonzalez de Vicente, Y. Wang, Ion beam analysis of fusion plasma-facing materials and components: facilities and research challenges, Nucl. Fusion 60 (2020) 025001, http://dx.doi.org/10.1088/1741-4326/ab5817.

[28] K. Kantre, P. Szabo, M.V. Moro, C. Cupak, R. Stadlmayr, L. Zendejas Medina, F. Aumayr, D. Primetzhofer, Combination of in-situ ion beam analysis and thermal desorption spectroscopy for studying deuterium implanted in tungsten, Phys. Scr. 96 (2021) 124004, http://dx.doi.org/10.1088/1402-4896/ac1a88.

[29] P. Ström, P. Petersson, M. Rubel, G. Possnert, A combined segmented anode gas ionization chamber and time-of-flight detector for heavy ion elastic recoil detection analysis, Rev. Sci. Instrum. 87 (2016) 103303, http://dx.doi.org/10.1063/1.4963709.

[30] K. Kantre, M.V. Moro, D. Moldaev, D. Johansson, D. Wessmann, M. Wolff, D. Primetzhofer, SIGMA: A set-up for in-situ growth, material modification and analysis by ion beams, Nucl. Instrum. Methods Phys. Res. B. 463 (2020) 96–100, http://dx.doi.org/10.1016/j.nimb.2019.11.007.

[31] P. Ström, D. Primetzhofer, Ion beam tools for nondestructive in-situ and in-operando composition analysis and modification of materials at the Tandem Laboratory in Uppsala, J. Instrum. 17 (2022) P04011, http://dx.doi.org/10.1088/1748-0221/17/04/P04011.

[32] K. Kantre, Materials analysis using MeV-ions: fundamental challenges and in-situ applications (Ph.D. thesis), Uppsala University, 2021.

[33] D. Rapp, P. Englander-Golden, D. Briglia, Cross sections for dissociative ionization of molecules by electron impact, J. Chem. Phys. 42 (1965) 4081, http://dx.doi.org/10.1063/1.1695897.

[34] A. Mutzke, A. Schneider, W. Eckstein, R. Dohmen, K. Schmid, U. von Toussaint, G. Bandelow, IPP report sdtrimsp version 6.00, in: Max-Planck-Institut FÜR Plasmaphysik, Tech. rep., 2019, URL https://pure.mpg.de/rest/items/item_3026474/component/file_3028154/content.

[35] P. Szabo, D. Weichselbaum, H. Biber, C. Cupak, A. Mutzke, R. Wilhelm, F. Aumayr, Graphical user interface for sdtrimsp to simulate sputtering, ion implantation and the dynamic effects of ion irradiation, Nucl. Instrum. Methods Phys. Res. B. 522 (2022) 47–53, http://dx.doi.org/10.1016/j.nimb.2022.04.008.

[36] M.V. Moro, R. Holeňák, L. Zendejas Medina, U. Jansson, D. Primetzhofer, Accurate high-resolution depth profiling of magnetron sputtered transition metal alloy films containing light species: A multi-method approach, Thin Solid Films 686 (2019) 137416, http://dx.doi.org/10.1016/j.tsf.2019.137416.

[37] J. Leavitt, L. McIntyre Jr., M. Ashbaugh, J. Oder, Z. Lin, B. Dezfouly-Arjomandy, Cross sections for 170.5° backscattering of ^{4}He from oxygen for ^{4}He energies between 1.8 and 5.0 MeV, Nucl. Instrum. Methods Phys. Res. B. 44 (1990) 260–265, http://dx.doi.org/10.1016/0168-583X(90)90637-A.

[38] M. Mayer, SIMNRA, a simulation program for the analysis of NRA, RBS and ERDA, AIP Conf. Proc. 475 (1999) 541, http://dx.doi.org/10.1063/1.59188.

[39] J. Ziegler, Official SRIM website, accessed 2022-04-05, 2022, URL http://srim.org/.

[40] A. Gurbich, SigmaCalc recent development and present status of the evaluated cross-sections for IBA, Nucl. Instrum. Methods Phys. Res. B. 371 (2016) 27–32, http://dx.doi.org/10.1016/j.nimb.2015.09.035.
[41] Z. Han, W. Hao, C. Wang, L. Shi, Elastic recoil cross section determination of deuterium by helium-4 ions at 30° with the energy range of 2.6–7.4 MeV, Nucl. Instrum. Methods Phys. Res. B. 375 (2016) 13–16, http://dx.doi.org/10.1016/j.nimb.2016.03.014.
[42] The J.E.T. Team, Results of JET operation with beryllium, J. Nucl. Mater. 176–177 (1990) 3–13, http://dx.doi.org/10.1016/0022-3115(90)90024-H.
[43] U. Wdowik, Structural stability and thermal properties of BeO from the quasi-harmonic approximation, J. Phys. Condens. Matter 22 (2010) 045404, http://dx.doi.org/10.1088/0953-8984/22/4/045404.
[44] J. Hlavac, Melting temperatures of refractory oxides: Part I, Pure Appl. Chem. 54 (1982) 681–688, http://dx.doi.org/10.1351/pac198254030681.
[45] R. Macaulay-Newcombe, D. Thompson, W. Smeltzer, Deuterium diffusion, trapping and release in ion-implanted beryllium, Fusion Eng. Des. 18 (1991) 419–424, http://dx.doi.org/10.1016/0920-3796(91)90158-M.
[46] R. Anderl, R. Causey, J. Davis, R. Doerner, G. Federici, A. Haasz, G. Longhurst, W. Wampler, K. Wilson, Hydrogen isotope retention in beryllium for tokamak plasma-facing applications, J. Nucl. Mater. 273 (1999) 1–26, http://dx.doi.org/10.1016/S0022-3115(99)00022-7.